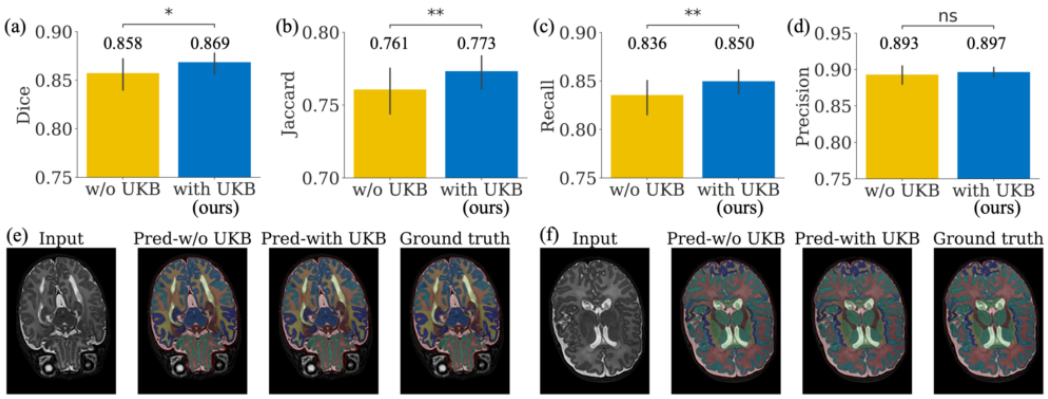

Figure 2. Quantitative and qualitative comparison of the foundation model (SwinUNETR with UKB pretraining) and SwinUNETR without UKB pretraining. Figure 2a-2d shows the bar plot comparisons of Dice score, Jaccard index, Recall and Precision. Figure 2e-2f shows the visual comparison of input MRI, prediction results of SwinUNETR without UKB pretraining, prediction results of SwinUNETR with UKB pretraining, and ground truth segmentations. The images are different slices from the same subject. Abbreviation and *p*-value annotation: ns = not significant; * = 1.00e-02 < p <= 5.00e-02; ** = 1.00e-03 < p <= 1.00e-02; w/o = without; pred = prediction; UKB = UK Biobank dataset.

Conclusions: This study highlights the strength of the foundation model, leveraging the brain anatomy knowledge gained from large-scale adult datasets, to improve prediction accuracy, segmentation stability, training convergence and generalisability across the lifespan.

References

1. Cabezas, M., Oliver, A., Lladó, X., Freixenet, J., & Bach Cuadra, M. (2011). A review of atlas-based segmentation for magnetic resonance brain images. Computer Methods and Programs in Biomedicine, 104(3), e158–e177. https://doi.org/10.1016/j.cmpb.2011.07.015
2. Cox, J., Liu, P., Stolte, S. E., Yang, Y., Liu, K., See, K. B., Ju, H., & Fang, R. (2024). BrainSegFounder: Towards 3D foundation models for neuroimage segmentation. Medical Image Analysis, 97, 103301. https://doi.org/10.1016/j.media.2024.103301
3. Makropoulos, A., Robinson, E. C., Schuh, A., Wright, R., Fitzgibbon, S., Bozek, J., Counsell, S. J., Steinweg, J., Vecchiato, K., Passerat-Palmbach, J., Lenz, G., Mortari, F., Tenev, T., Duff, E. P., Bastiani, M., Cordero-Grande, L., Hughes, E., Tusor, N., Tournier, J.-D., … Rueckert, D. (2018). The developing human connectome project: A minimal processing pipeline for neonatal cortical surface reconstruction. NeuroImage, 173, 88–112. https://doi.org/10.1016/j.neuroimage.2018.01.054
4. Segment anything in medical images | Nature Communications. (n.d.). Retrieved March 3, 2025, from https://www.nature.com/articles/s41467-024-44824-z
5. Shen, D. D., Bao, S. L., Wang, Y., Chen, Y. C., Zhang, Y. C., Li, X. C., Ding, Y. C., & Jia, Z. Z. (2023). An automatic and accurate deep learning-based neuroimaging pipeline for the neonatal brain. Pediatric Radiology, 53(8), 1685–1697. https://doi.org/10.1007/s00247-023-05620-x
6. Sun, Y., Gao, K., Wu, Z., Li, G., Zong, X., Lei, Z., Wei, Y., Ma, J., Yang, X., Feng, X., Zhao, L., Le Phan, T., Shin, J., Zhong, T., Zhang, Y., Yu, L., Li, C., Basnet, R., Ahmad, M. O., … Wang, L. (2021). Multi-Site Infant Brain Segmentation Algorithms: The iSeg-2019 Challenge. IEEE Transactions on Medical Imaging, 40(5), 1363–1376. IEEE Transactions on Medical Imaging. https://doi.org/10.1109/TMI.2021.3055428
7. Tang, Y., Yang, D., Li, W., Roth, H. R., Landman, B., Xu, D., Nath, V., & Hatamizadeh, A. (2022). Self-Supervised Pre-Training of Swin Transformers for 3D Medical Image Analysis. 20730–20740. https://openaccess.thecvf.com/content/CVPR2022/html/Tang_Self-Supervised_PreTraining_of_Swin_Transformers_for_3D_Medical_Image_Analysis_CVPR_2022_paper.html
8. The UK Biobank imaging enhancement of 100,000 participants: Rationale, data collection, management and future directions | Nature Communications. (n.d.). Retrieved March 3, 2025, from https://www.nature.com/articles/s41467-020-15948-9

Poster No 1656

Attention-gated Convolutional Neural Network for Automated Segmentation of Fetal Subplate from MRI

Andrea Gondova[1], Milton O. Candela-Leal[1], Hyuk Jin Yun[1], Sungmin You[1], Seungyoon Jeong[1], Marisol Aguilar[1], P. Ellen Grant[1], Kiho Im[1]

[1]Fetal Neonatal Neuroimaging and Developmental Science Center, Boston Children's Hospital, Boston, MA

Introduction: The subplate (SP) is a transient fetal brain structure implicated in numerous developmental processes, including neuronal migration, circuit formation, and early cortical activity, with its alterations linked to neurodevelopmental disorders (Kostović, 2020). While recent advances in fetal MRI enable in vivo SP visualization, automated segmentation — crucial for large-scale, non-invasive studies — remains underexplored compared to other brain structures like the cortical plate (CP) (Dou et al., 2020; Uus et al., 2023). To address this gap, we extend a validated attention-gated U-Net model (Hong et al., 2020), originally developed for CP segmentation, to incorporate SP to facilitate a more comprehensive fetal brain analysis.

Methods: We analyzed a retrospective multi-site cohort of T2-weighted fetal brain MRI from 134 typically developing fetuses (GW: 27.32 ± 2.67, range: 21.86–31.86). Data processing included brain masking, slice-to-volume registration, alignment to a 31-week template (You et al., 2024), and N4 bias field correction to mitigate scanner variations (Tutison et al., 2010). Fourteen cases were held out for testing, while 120 were used for training and validation (Figure 1a,b). Our approach consisted of an ensemble of three 2D Attention Gated U-Net models trained on axial, coronal, and sagittal planes, with multi-view aggregation and test-time augmentation (MVA-TTA) to improve segmentation stability. A hybrid loss function combining Dice and focal loss was used to enhance boundary delineation (Hong et al., 2020)(Figure 1c).

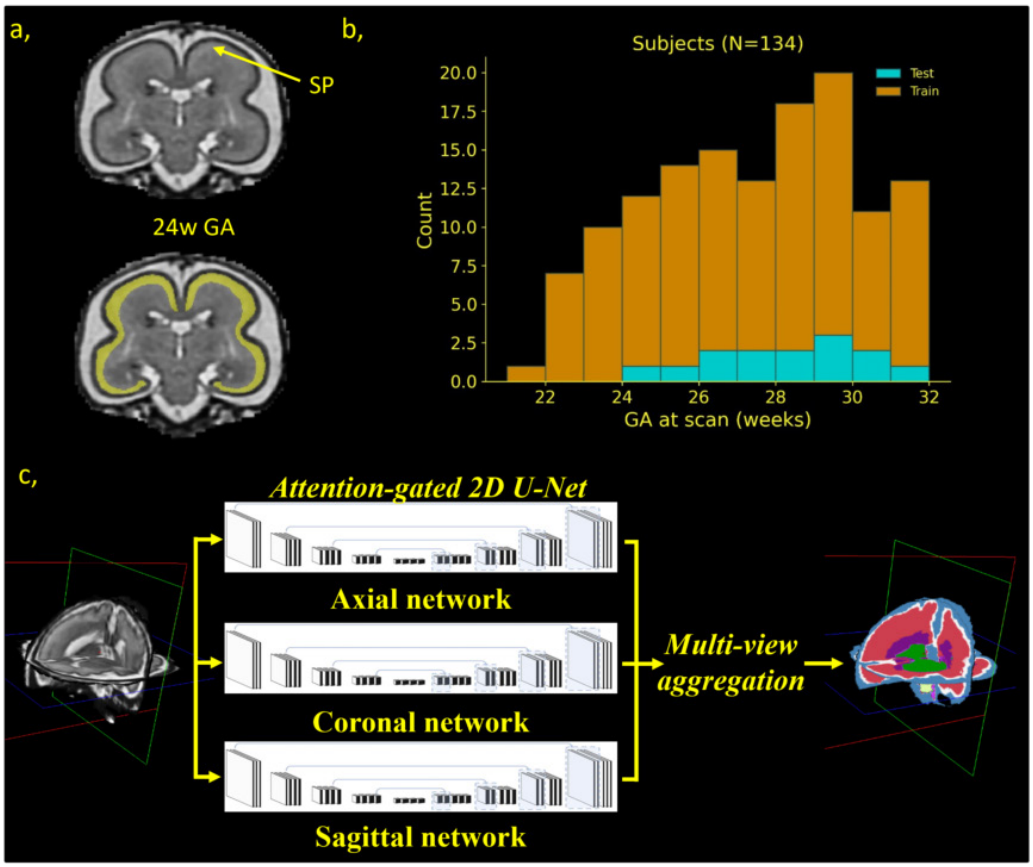

Figure 1a, 3D reconstruction of fetal T2-weighted MRI with SP visible as a hyperintense band beneath the cortical plate. Manual segmentation is highlighted in yello. **b,** Subject age distribution across training and testing sets. The 32-week GA upper limit was chosen as SP contrast becomes indistinguishable from the intermediary zone in T2-weighted MRI[7]. **c,** Attention-gated U-Net-based network architecture incorporating multi-view aggregation with test-time augmentation. Three separately trained models (axial, coronal, sagittal) are combined using majority voting to enhance segmentation stability and accuracy.

Results: Our model demonstrated high segmentation performance, achieving a global Dice score of 0.98 ± 0.015 (mean ± std), Hausdorff distance of 5.36 ± 2.406 voxels, and 1.29 ± 0.929% volumetric change in the test set. Performance was consistent across tissue types. We observed a slight (non-significant) decline increasing gestational age, likely due to evolving tissue contrast and morphology complexity (Figure 2a). Qualitative evaluations showed most segmentation errors at the CP/SP boundary (Figure 2b). Despite these, our method provided sufficient accuracy for volumetric and morphometric SP analyses, significantly reducing the need for extensive manual correction in follow-up studies (data not shown).

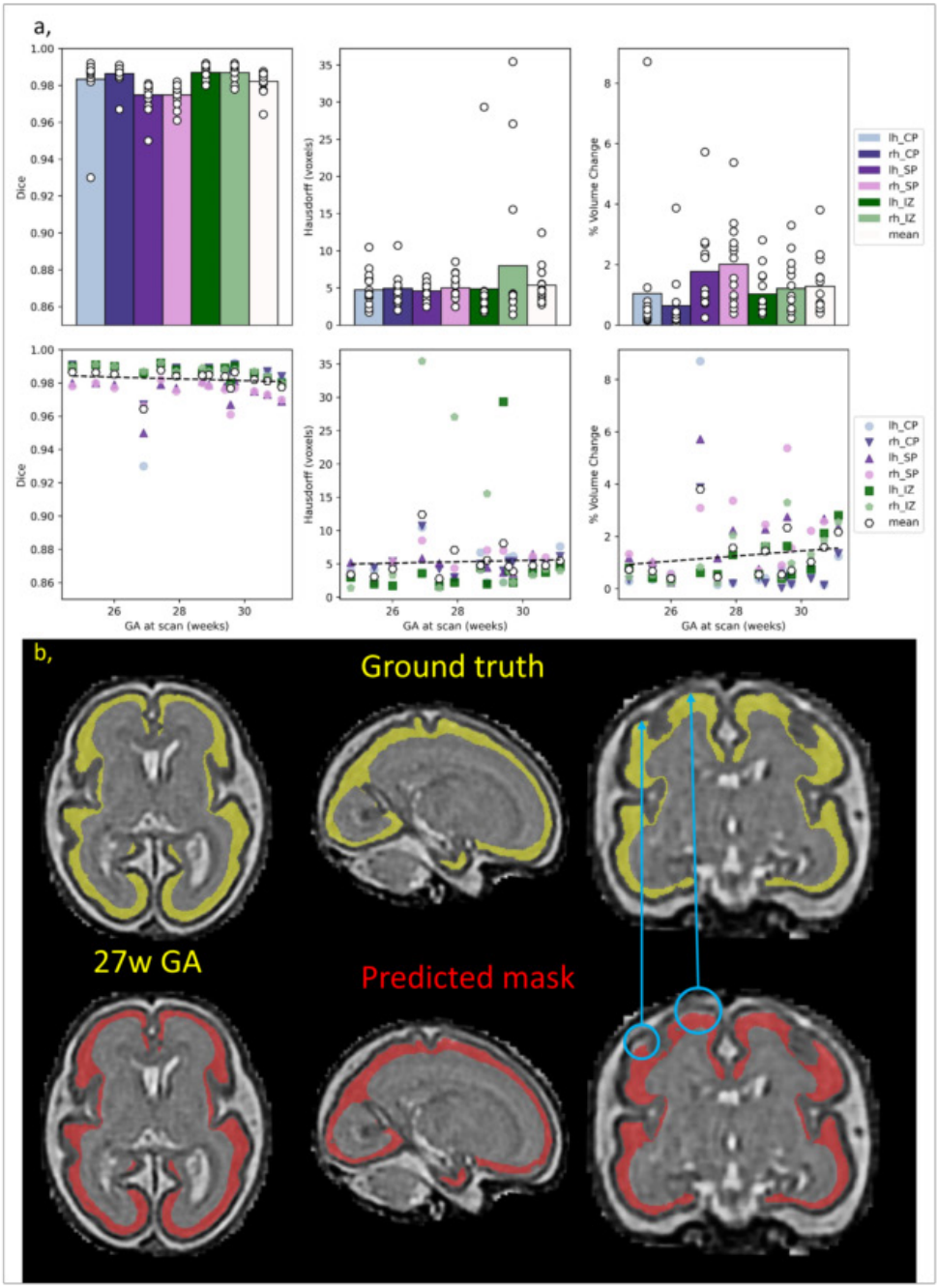

Figure 2a, Model performance in the testing set (n=14). The top row shows segmentation quality metrics—Dice coefficient, Hausdorff distance, and % Volumetric Change—across different tissues. Bars indicate mean values, with individual subject data points overlaid. The bottom row illustrates tissue-wise performance relative to gestational age, with a dotted linear fit (not significant). **b,** Ground truth manual segmentation (yellow) vs. model-predicted SP segmentation (red) for the lowest-performing subject (27w GA). Blue circles highlight most common errors, primarily at the CP/SP boundary.

Conclusions: We present an automated deep-learning approach for automated SP segmentation in fetal MRI, expanding existing method for large-scale studies of typical and atypical SP development. While minor manual correction remains necessary, particularly in low-quality scans or complex morphologies at later gestational stages, future improvements could incorporate automated refinement techniques such as conditional random fields (Chen et al., 2021) or hybrid segmentation approaches (Gaset et al., 2024). By reducing reliance on labor-intensive manual segmentation, this work will allow future work that could enhance the study of in utero brain development, advance our understanding of early brain development and detect early biomarker for various clinical populations with adverse neurodevelopmental outcomes.

References
1. Chen, S., Sedghi Gamechi, Z., Dubost, F., van Tulder, G., & de Bruijne, M. (2021). An end-to-end approach to segmentation in medical images with CNN and posterior-CRF. Medical image analysis, 76, 102311
2. Diogo, M. C., Prayer, D., Gruber, G. M., Brugger, P. C., Stuhr, F., Weber, M., Bettelheim, D., & Kasprian, G. (2019). Echo-planar FLAIR Sequence Improves Subplate Visualization in Fetal MRI of the Brain. Radiology, 292(1), 159–169
3. Dou, H., Karimi, D., Rollins, C.K., Ortinau, C.M., Vasung, L., Velasco-Annis, C., Ouaalam, A., Yang, X., Ni, D., & Gholipour, A. (2020). A Deep Attentive Convolutional Neural Network for Automatic Cortical Plate Segmentation in Fetal MRI. IEEE Transactions on Medical Imaging, 40, 1123-1133.
4. Gaser Ch., Dahnke R., (2024) CAT faces Python – Combining Deep-Learning with Traditional Segmentation. OHBM 2024 Annual Meeting, Seoul, South Korea.
5. Hong, J., Yun, H.J., Park, G., Kim, S., Laurentys, C.T., Siqueira, L.C., Tarui, T., Rollins, C.K., Ortinau, C.M., Grant, P.E., Lee, J., & Im, K. (2020). Fetal Cortical Plate Segmentation Using Fully Convolutional Networks With Multiple Plane Aggregation. Frontiers in Neuroscience, 14.
6. Kostović, I. (2020). The enigmatic fetal subplate compartment forms an early tangential cortical nexus and provides the framework for construction of cortical connectivity. Progress in Neurobiology, 194.
7. Tustison, N., Avants, B.B., Cook, P.A., Zheng, Y., Egan, A., Yushkevich, P., & Gee, J.C. (2010). N4ITK: Improved N3 Bias Correction. IEEE Transactions on Medical Imaging, 29, 1310-1320.
8. Uus, A. U., Kyriakopoulou, V., Makropoulos, A., Fukami-Gartner, A., Cromb, D., Davidson, A., Cordero-Grande, L., Price, A. N., Grigorescu, I., Williams, L. Z. J., Robinson, E. C., Lloyd, D., Pushparajah, K., Story, L., Hutter, J., Counsell, S. J., Edwards, A. D., Rutherford, M. A., Hajnal, J. V., & Deprez, M. (2023). BOUNTI: Brain vOlumetry and aUtomated parcellatioN for 3D feTal MRI. eLife 12:RP88818.
9. You, S., Barba, A.D., Tamayo, V.C., Yun, H.J., Yang, E., Grant, P.E., Im, K., Wu, Z., Zhao, F., Leon, D., Tamayo, C., Yun, H., & Grant, P.E. (2024). Automatic cortical surface parcellation in the fetal brain using attention-gated spherical U-net. Frontiers in Neuroscience, 18.

Poster No 1657

Mapping fMRI-BOLD nonlinear dynamics to transcriptional gradients via Koopman similarity analysis

Nghi Nguyen[1], Jingxuan Bao[2], Jiong Chen[2], Trang Cao[3], Bojian Hou[2], Shu Yang[2], Yize Zhao[4], Christos Davatzikos[2], Li Shen[2], Duy Duong-Tran[2]

[1]Vrije Universiteit Amsterdam, Amsterdam, The Netherlands, [2]Perelman School of Medicine, University of Pennsylvania, Philadelphia, PA, [3]Monash Biomedical Imaging, Monash University, Clayton, Victoria, [4]School of Public Health, Yale University, New Haven, CT

Introduction: Human brain functions are increasingly understood through gradients derived from fMRI-BOLD via diffusion mapping (Bernhardt, 2022). While effective at capturing macro-scale functional connectivity and its alignment with the spatial distribution of 24 cell types (Zhang, 2024), it remains unclear how this approach elucidates the emergence of the macroscopic BOLD variance that cannot be explained by these broad cell types alone. We propose that diffusion mapping using linear correlations overlooks associations with finer neurobiological variations. Using similarity analysis of Koopman operators (Kamiy, 2024; Ostrow, 2024), we show that nonlinear BOLD features strongly align with transcriptional gradients of numerous genes, clusters of which are enriched in functions underpinning macroscopic BOLD variance.

Methods: We used resting-state fMRI data from the Max Planck Institute Leipzig Mind-Brain-Body Dataset (LEMON) (Babayan, 2019), preprocessed by Jimenez-Marin et al. (2024). For alignment with transcriptomic data from the Allen Human Brain Atlas (Shen, 2012), fMRI images were parcellated into 391 regions using the Initial Parcellation Atlas (Jimenez-Marin, 2024). Participants aged 20–30 were split into two groups: one (30 subjects) for hyperparameter tuning and another (106 subjects) for analysis. For each subject, Koopman operators were estimated for 391 BOLD time courses using a Nystroem-accelerated RBF approach (Meanti, 2024). Pairwise L2-Wasserstein distances between the singular value spectra of Koopman estimators yielded a 391-by-391 distance matrix M per subject, which embeds nonlinear BOLD dynamics. Hyperparameters of the estimators were tuned by minimizing normalized eigenvalue sums (NeSUM) of each embedding matrix M (He, 2022). Principal components (PCs) of the group-averaged embedding were extracted using multidimensional scaling. We assessed alignment between each PC and gene transcription via Spearman correlation, testing significance with a spatially constrained Moran spectral randomization. Genes with Bonferroni-corrected significance were used to construct an interaction network with STRING, where clusters were identified by Louvain community detection. We manually labeled each cluster using the Gene Ontology (GO) enrichment terms assigned to its constituent genes.

Results: We identified three PCs of the embedding manifold, each roughly organizing the brain along a major functional axis described in previous studies (Cross, 2021): Multiple Demand-Limbic, Transmodal-Sensory, and Somatomotor-Visual (Figure 1A, B, C). The Transmodal-Sensory axis significantly aligned with 667 genes, forming 26 clusters significantly enriched in GO processes linked to neurotransmission, cell morphology, and neurovascular coupling (Figure 1D, E). The other PCs showed weaker alignment with gene expression: the Multiple Demand-Limbic axis is correlated with just 6 genes, and the Somatomotor-Visual axis with 36 genes. Applying the same transcriptomic alignment to diffusion mapping eigenvectors from the functional connectome (via the Pearson correlation matrix) showed far fewer significant gene correlations: 6, 18,